Efficient Pro-survival/angiogenic miRNA Delivery by an MRI-Detectable Nanomaterial

Renata S. M. Gomes,[†,‡,§,⊥,∥] Ricardo Pires das Neves,[†,‡] Lowri Cochlin,[⊥,¶] Ana Lima,[†,‡,¶] Rui Carvalho,[‡] Petra Korpisalo,[∥] Galina Dragneva,[∥] Mikko Turunen,[∥] Timmo Liimatainen,[∥] Kieran Clarke,[⊥] Seppo Ylä-Herttuala,[∥] Carolyn Carr,[⊥] and Lino Ferreira[†,‡,*]

[†]CNC, Center for Neuroscience and Cell Biology, University of Coimbra, 3004-517 Coimbra, Portugal, [‡]Biocant, Center of Innovation in Biotechnology, 3060-197 Cantanhede, Portugal, [§]Cardiovascular Biology & Medicine, Rayne Institute, University College, London, U.K., [⊥]Cardiac Metabolism Research Group, Department of Physiology, Anatomy & Genetics, University of Oxford, U.K., and [∥]A.I. Virtanen Institute, Department of Biotechnology and Molecular Medicine, University of Eastern Finland, Finland. [¶]These authors contributed equally to this manuscript.

ABSTRACT Herein, we report the use of biodegradable nanoparticles (NPs) containing perfluoro-1,5-crown ether (PFCE), a fluorine-based compound (NP170-PFCE) with the capacity to track cells *in vivo* by magnetic ressonance imaging (MRI) and efficiently release miRNA. NP170-PFCE complexed with miRNAs accumulate whitin the cell's endolysosomal compartment and interact with higher frequency with argonaute2 (Ago2) and GW182 proteins, which are involved in the biological action of miRNAs, than commercial complexes formed by commercial reagents and miRNA, which in turn accumulate in the cell cytoplasm. The release of miRNA132 (miR132) from the NPs increased 3-fold the survival of endothelial cells (ECs) transplanted *in vivo* and 3.5-fold the blood perfusion in ischemic limbs relatively to control.

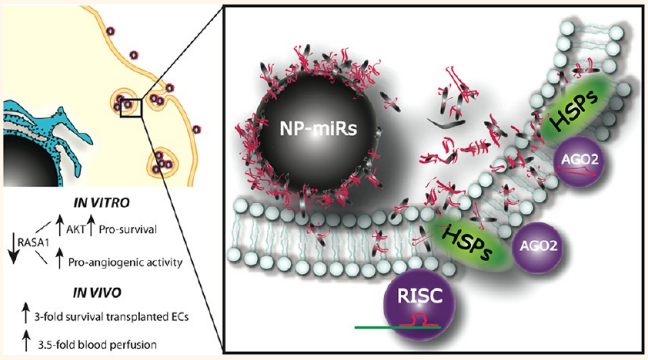

KEYWORDS: nanoparticles · MRI · miRNA · cell tracking · ischemic diseases

Several pro-angiogenic strategies have been proposed in the past years for the treatment of ischemic diseases, including growth factor delivery, cell-based therapies, and gene therapies. Cell-based therapies, specifically the ones based on the use of vascular cells, hold high promise, as they can contribute simultaneously to the formation of neovessels and secretion of angiogenic factors. Unfortunately, most transplanted cells die a few days after delivery.[1,2] Cell modulation by miRNAs has been recently tested as a strategy to enhance cell survival and pro-angiogenic activity.[3−5] MiRNAs are noncoding single-strand RNAs that post-transcriptionally regulate gene expression.[6] In comparison to classical drugs, individual miRNAs can regulate many target genes and influence a whole gene network. Strategies have been reported for the *in vivo* delivery of miRNAs, including (i) chemical modification, (ii) liposomes, (iii) adeno-associated virus or lentivirus, and (iv) biodegradable NPs.[7−10] Unfortunately, there is no formulation for the delivery of miRNA that simultaneously offers control of intracellular location and the possibility to track the transfected cells. This technology would offer high efficiency in the regulatory mechanism of miRNAs and the possibility of monitoring cells transplanted into ischemic tissues by the use of noninvasive imaging techniques such as magnetic resonance imaging (MRI).[11]

Studies on miRNA delivery have explored NPs that accumulate in the cytoplasm and not in the endolysosomal compartment,[12,13] as it was believed that RNA regulation occurred largely within the cytoplasmic, membrane-free cellular regions.[14] In the cytoplasm, Ago proteins bind to Dicer, which are able to interact with the miRNA duplex and induce the removal of one of the miRNA strands. The complex Ago−miRNA is then ready to bind target mRNA.[14] However, recent data indicate that RNA regulation occurs in the endolysosomal compartments.[14,15] Many RNA

* Address correspondence to lino@biocant.pt.

Received for review January 12, 2013 and accepted March 2, 2013.

Published online March 03, 2013
10.1021/nn400171w

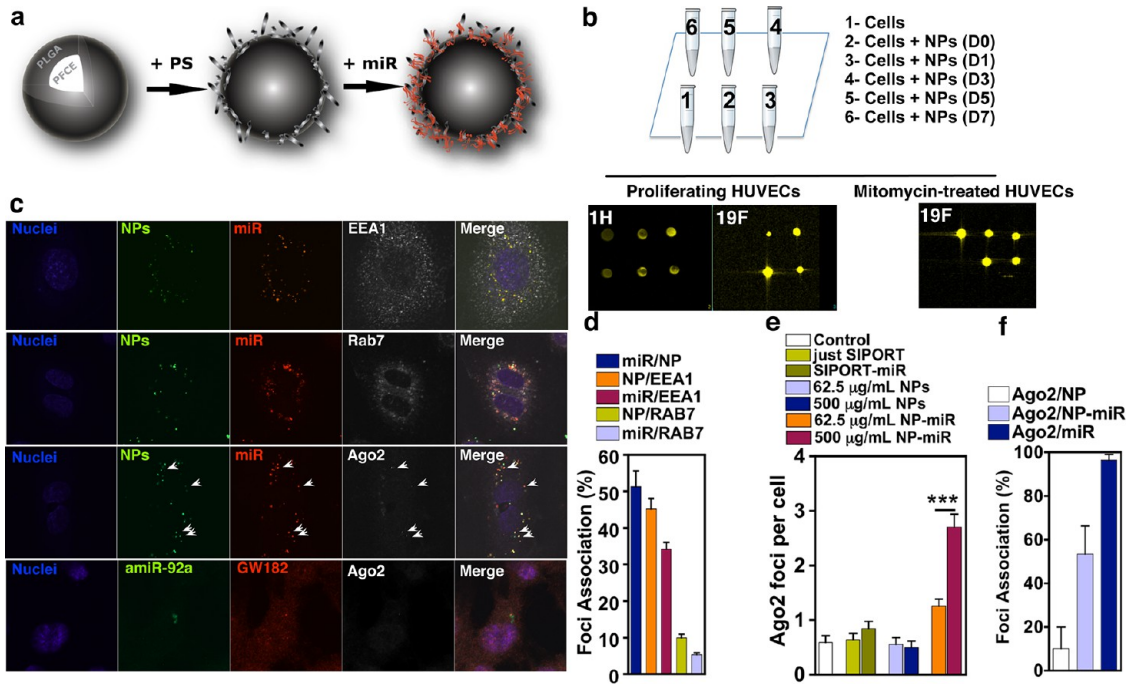

Figure 1. Cell tracking and NP170-mediated delivery of miRNAs. (a) Schematic representation of NP preparation. The NPs are formed by PLGA encapsulating PFCE. The NP is then coated with PS, which has a dual role: (i) to facilitate cell internalization and (ii) to mediate the complexation of miRNAs. (b) ^{19}F signal during cell proliferation. MR images of Eppendorf tubes containing unlabeled cells in PBS or cells transfected with NP170-PFCE (10×10^6 cells in both) at day 0 (D0), 1 (D1), 3 (D3), 5 (D5), and 7 (D7) after labeling, with or without treatment with mitomycin. Eppendorf tubes were positioned in a support inside a ^{19}F/^{1}H MRI volume coil in a 7 T magnet. The acquisition time was 10 min (5 averages) for 10×10 cm, matrix 256×256, TR = 500 ms, flip angle 50°. (c) Representative images of the intracellular distribution of NP-PFCE-FITC (NPs) and miR-DY547 (miR) in relation to the early endosome (EEA1) and late endosome/lysosome (Rab7) vesicles (top panels) and the association between NP and miR-Dy547 foci with Ago2 (bottom panels). The amiR-92a associates with both GW182 and Ago2 proteins. (d) Intracellular localization of NP and miR-Dy547 foci in relation to the endomembrane system. It is presented as the number of foci inside the cell (% from the total), which are interacting with the species in the denominator. (e) Quantification of the number of Ago2 foci present inside the cell under different transfection conditions showing that the number of Ago2 foci present in the cell increases with increased concentrations of NPs carrying miR-Dy547. ***$p < 0.001$. (f) Analysis of Ago2 association profile in NP170-PFCE/miR-Dy547-transfected cells. Quantification of the degree of association of Ago2 foci and NP-only foci (Ago2/NP), NP foci and miR foci (Ago2/NP-miR), and foci containing only miR (Ago2/miR). In c, d, e, and f, the analyses were performed at 24 h after cell transfection.

processes may be spatially restricted in the endolysosomal compartments to promote specificity and kinetic efficiency.[16] Thus far, no NP formulation has been shown to accumulate in the endolysosomal compartment and efficiently release the miRNA.

Here we report a novel NP formulation that can be used simultaneously for cell tracking and miRNA delivery. The NP core was formed of poly(lactic acid-*co*-glycolic acid) (PLGA) and PFCE,[17,18] a fluorine compound that can be tracked noninvasively by ^{19}F MRI (Figure 1a). PFCE contains 20 equivalent ^{19}F spins that generate a single resonance in NMR imaging (Figure S1) and it is relatively noncytotoxic.[19] ^{19}F MRI can selectively image transplanted cells labeled with NP170-PFCE formulation since no fluorine exists within the human body. The NPs were further coated with protamine sulfate (PS), a polycationic peptide that has been shown to efficiently condense plasmid DNA.[20] All NP components are FDA-approved for biomedical applications.[21] We show that endothelial and mononuclear cells can rapidly internalize the NPs, which largely remained within the endolysosomal compartment. Most importantly, the NPs mediated the intracellular delivery of miR132, which subsequently exerted a pro-survival effect in cells exposed to hypoxia, both in *in vitro* and *in vivo* models. Finally, we demonstrated the possibility of tracking the transplanted cells with ^{19}F MRI.

RESULTS AND DISCUSSION

Engineering NPs for Cell Labeling. PLGA NPs without PFCE had an average diameter of 170 nm and a negative (*ca.* −9 mV) zeta potential (Table S1). The PFCE encapsulation within the NPs increased their average diameter from 170 nm to 213 nm. ^{19}F NMR analysis demonstrated the encapsulation efficiency was between 4.9% and 13.8% (Table S2). The NP170-PFCE formulation contained between 111.0 and 176.5 μg of PFCE per mg of PLGA. To facilitate the NP170-PFCE intracellular delivery and the loading of miRNA, the NPs were coated with PS, a small cationic agent (Table S3).[22] The NPs were relatively stable at intracellular pHs and, in concentrations up to 1 mg/mL, did not exert substantial cytotoxicity to human umbilical vein endothelial cells (HUVECs) or mononuclear cells (MNCs) (Figures S1 and S2).

To characterize the intracellular delivery of NP170-PFCE into the cytoplasm of HUVECs or MNCs, we performed confocal microscopy analyses. The NPs were labeled with fluoresceinimine as a reporter to follow NP delivery in cells. Both cell types were incubated with 500 μg/mL of NPs for 4 h in serum-free media. NPs were internalized by HUVECs and accumulated in the endolysosomal compartment (Figure S3). Endosomal sequestration persisted up to 144 h following incubation, indicating relatively little self-mediated escape or disruption of endosomal membranes by the NPs themselves. Similar results were obtained for MNCs (Figure S3).

To quantify cell-labeling efficiency under the different conditions, we performed fluorescence activated cell sorting (FACS) and ^{19}F NMR. Cells were incubated with NPs at concentrations between 0.5 and 4 mg/mL for 4 h, washed to remove loosely bound particles, and then characterized by FACS. When 500 μg/mL of NP170-PFCE-PS was incubated with cells, 65% (HUVECs) and 80% (MNCs) of the cells were labeled after 4 h (Figure S2). ^{19}F NMR measurements indicated that this labeling corresponded to the internalization of 0.27 (HUVECs) and 0.15 ng (MNCs) of PFCE per cell, which was sufficient for cells to be detected on a ^{19}F 7T MRI volume coil (Figure 1b). As expected, the PS-coated NP170-PFCE formulation was taken up by cells at a higher rate (approximately 2 times) than uncoated ones (Figure S2).

Long-term observation of NP170-PFCE-labeled cells could be limited by the dilution of NPs following cell division. Therefore, we quantified cell NP labeling over time using MRI (Figure 1b). HUVECs were labeled with NPs for 4 h, and the labeled cell population was isolated by cell sorting and cultured for 7 days in EGM-2 medium. During this time, cells proliferated and the percentage of NP170-PFCE-labeled cells decreased over time, being undetected by ^{19}F MRI at day 7 (*ca.* four cell doublings). When the cell cycle was inhibited by mitomycin, the intracellular level of NPs remained fairly constant over 7 days, confirming that the decrease in the proportion of NP-labeled cells was due to cell division (Figure 1b).

Intracellular Release of miRNA. Next, we tested whether NP170-PFCE could be used to deliver pro-survival miRNAs such as miR132, miR424, and antagomir-92a (amiR92a) within cells. MiR132 has been reported to induce EC proliferation and tube formation in a three-dimensional collagen matrix.[9] miR424 stabilizes hypoxia-inducible factor 1α and plays an important physiological role in postischemic vascular remodeling and angiogenesis.[23] AmiR92a induces angiogenesis *in vitro* and *in vivo* by regulating the expression of the integrin subunit α5.[4]

To investigate the internalization of miRNAs by the cells, Dy547-labeled miRNA was complexed with FITC-labeled NP170-PFCE for 1 h (under these conditions, 12 μg of miRNA was complexed per mg of NPs), washed, and then incubated with HUVECs for 4 h. Dy547-labeled miRNA is a mimic microRNA without any human targets (no fluorescent miR132 and miR424 could be obtained commercially). Cells were washed with PBS to remove NPs that were not internalized, and characterized by confocal microscopy. To evaluate the potential of our approach, we performed the same experiment using a commercial transfection agent, SIPORT NeoFX. The complex Dy547-miRNA/FITC-NP170-PFCE was highly internalized by cells, with over 90% of the cells transfected using NP170-PFCE/Dy547-miRNA, while only 50% of the cells were transfected using SIPORT/Dy547-miRNA (Figure S4). However, cells transfected using SIPORT had more Dy547-miRNA whitin the cell cytoplasm than those transfected using NP170-PFCE/Dy547-miRNA.

FITC-labeled NP170-PFCE formulation internalized by HUVECs was localized in restricted cell areas (Figure 1c). At 24 h post-transfection, ~50% of the miRNA co-localized with the NPs, thus showing that half of the miRNA had already been released by the NPs (Figure 1d). Approximately 35% of the miR-Dy547 foci were associated with early endosome vesicles (EEA1$^+$ vesicles), while only 5% were located in late endosome and lysosome vesicles (Rab7$^+$ vesicles). Overall, there was a low degree of association of both NP and miR with late endosome and lysosome vesicles. In contrast, the Dy547-miRNA released by SIPORT NeoFX was distributed across the cell cytoplasm and not within confined intracellular areas (Figure S5). Importantly, the NP170-PFCE formulation was able to present miRs to the RISC protein Ago2 more efficiently than SIPORT. NP delivery induced more Ago2 foci than SIPORT delivery (Figure 1e and f). The same was observed in cells transfected with fluorescent amiR-92a (Figure 1c). Amir-92a foci showed association with both Ago2 and GW182 proteins, indicating that this anti-miR oligonucleotide may be capable of microRNA-RISC strand invasion. Interestingly, the number of foci was higher in cells cultured under hypoxia than in normoxia, indicating higher efficiency for the biological effect of miRNA under these conditions (Figure 2).

Pro-survival and Pro-angiogenic Activity of the miRNA-Containing NPs. To demonstrate the pro-survival activity of different miRNAs, HUVECs were incubated for 4 h with miRNA-complexed NPs, washed, and finally cultured in ischemic conditions (pO_2 of 0.1%; media without serum) for 48 h. miR132, miR424, and amiR92a/NP170-PFCE formulations each significantly ($p < 0.05$, $n = 3$) increased cell survival, and this effect was dependent on the miRNA concentration (Figure 3a). No significant differences were seen between the different miRNAs tested ($p > 0.05$, $n = 3$). miRNAs delivered by the SIPORT transfection agent mediated cell survival only at concentrations higher than those that gave increased survival using NP170-PFCE.

To demonstrate the pro-angiogenic effects of the miRNA-containing NP formulations, HUVECs were

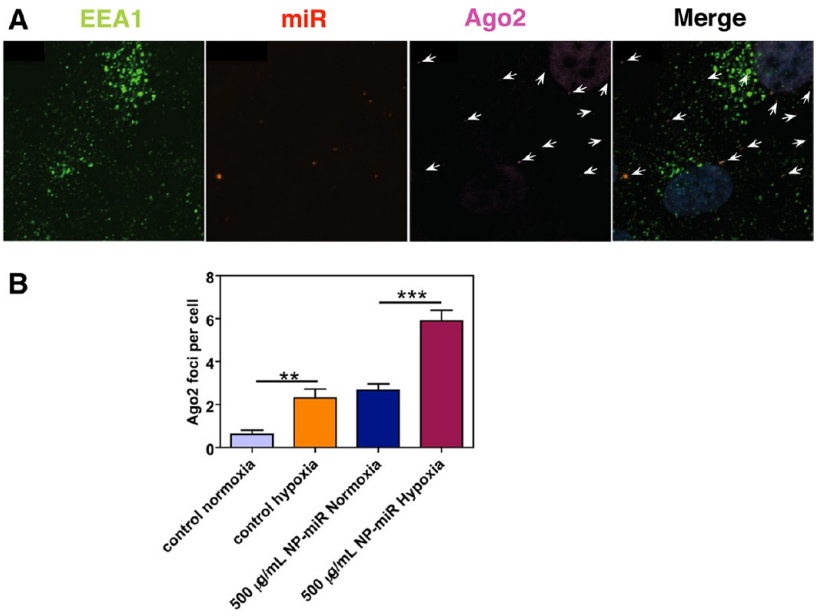

Figure 2. Effect of hypoxia in co-localization of miR with Ago2 and EEA1. HUVECs were transfected with NP170-PFCE/miR-Dy547 for 4 h, washed to remove NPs that were not internalized, and incubated for 24 h in hypoxia and serum-deprived conditions. (A) Confocal microscopy results showing the association of miR-Dy547 with Ago2 and the early endosome protein EEA1. (B) Quantification of Ago2 foci per cell. Representative microscopic fields were used for quantification spanning a total area of 3.8 mm^2 (approximately 120 cells were analyzed). Results are mean ± SEM (n = 8−18). $p \leq 0.01$ (**) and $p \leq 0.001$ (***).

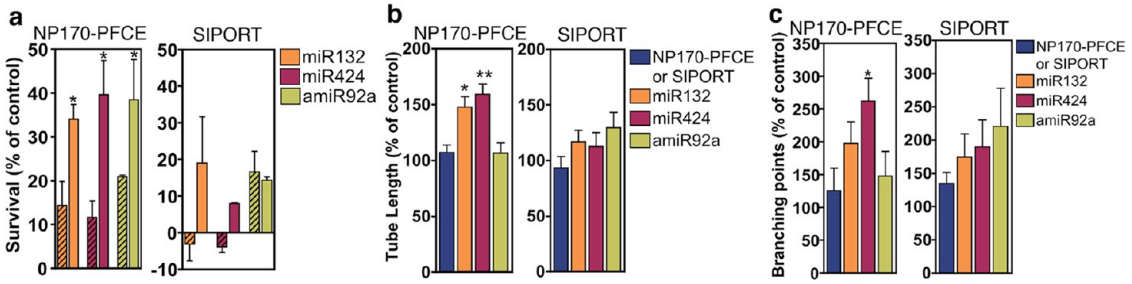

Figure 3. Pro-survival and pro-angiogenic effects of NP170-PFCE:miR complexes on ECs. (a) HUVEC survival under hypoxia and serum-deprived for 48 h as assessed by an ATP-based assay. NPs were complexed with 100 nM (stripe pattern) or 200 nM (no pattern) miR. (b, c) HUVECs treated with different formulations in normoxia were cultured in a Matrigel assay for 24 h, after which the tube length (b) or branching points (c) were measured. In all graphs, results are average ± SEM (n = 3). $p \leq 0.05$ (*) and $p \leq 0.01$ (**).

incubated for 4 h with miRNA-complexed NPs, washed, and finally cultured on top of Matrigel to assess their capacity to form vascular networks. The transfection of the cells with miR132- and miR424-containing NP170-PFCE yielded vascular networks with greater tube length and more branching points than cells transfected with SIPORT for the same miRNAs (Figure 3b and c).

From all the miRNAs tested, we selected miR132 for subsequent analysis. miR132 is expressed by ECs after 3−6 h of exposure to vascular endothelial growth factor or basic fibroblast growth factor.[9] In addition, the constitutive expression of miR132 in HUVECs considerably increases cell proliferation and tube formation. One of the identified targets of miR132 is RASA1, which encodes p120RasGAP. HUVECs transfected with miR132 have a decreased endogenous p120RasGAP expression, which increased Ras activity and mitogen-activated protein kinase extracellular related protein kinase-1 (MEK-1). To demonstrate that RASA1 was indeed downregulated in HUVECs transfected with NP170-PFCE/miR132, we have performed quantitative real-time polymerase chain reaction (qRT-PCR) (Figure 4a) and protein quantification by immunofluorescence analysis (Figure 4b). HUVECs were incubated for 4 h with NP170-PFCE/miR132 or NP170-PFCE/scrambled miR or only NP170-PFCE, followed by washing and evaluation of mRNA levels after 24 h and protein expression after 48 h. HUVECs transfected with NP170-PFCE/miR132 had a downregulation in the expression of RASA1 mRNA, while no effect was observed in control groups. Moreover, the NP-miR132 delivery was more effective in downregulating p120RasGAP protein levels than SIPORT.

Overall, our results obtained on pro-survival, pro-angiogenic, and molecular assays show that the NP170-PFCE formulation is able to present miRNAs very effectively to the RISC complex machinery, outperforming

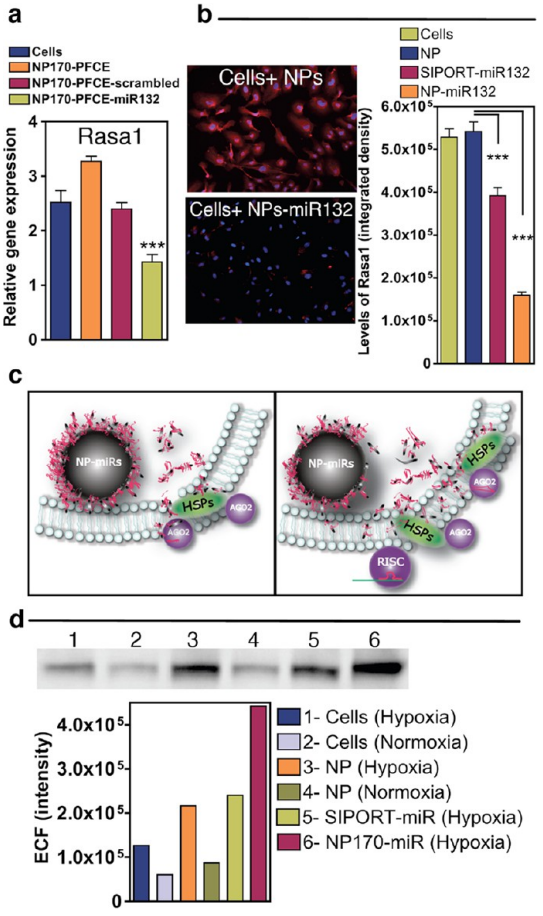

Figure 4. NP170-PFCE:miR-132 complexes target RASA1. (a) RASA1 gene expression in HUVECs treated with NP170-PFCE/scrambled miR or NP170-PFCE/miR132. Gene expression was normalized to GAPDH as a housekeeping gene. In all graphs, results show average ± SEM (n = 4). $p \leq 0.001$ (***). (b) RASA1 protein expression in HUVECs treated with different formulations. Levels of RASA1 (integrated density: average ± SEM) were measured with ImageJ after immunofluorescence and imaging of 10 representative fields (20× objective; ±300 cells). (c) Schematic representation of the translocation of miRNAs involving HSPs. (d) Immunoprecipitation of HSP90 and detection of Ago2 under different conditions by Western blot.

the commercial transfection system (SIPORT) in terms of Ago2 assembly, evidenced by an increased number of Ago2 foci with increasing NP-miR concentrations. We hypothesize that the better efficiency is related to the close association between the NP with the endomembrane system[14] (Figure 4c). The close relationship between the RISC machinery and the endomembrane system may promote frequent encounters with the exogenous oligonucleotides and NPs, while these encounters are reduced with SIPORT delivery, due to the diffusion and dilution of the oligonucleotides in the cytoplasm. Since Ago proteins are located in the membrane of the endolysosomal compartment,[14] and the miRNA binding site is located in the cytosolic part of the protein, the miRNA released from the NP has to cross the membrane of the endolysosomal compartment. This process may be mediated by the cationic NPs. Previous studies have shown that cationic NPs have the capacity to penetrate the endolysosomal membrane by generating transient holes and to rupture the endosomal vesicles by the well-known "proton sponge effect".[24] Alternatively, the miRNA release from the endolysosomal compartment may be mediated by Ago-chaperone heat shock proteins (HSPs), such as HSP90 and Hsc70,[25] which have been reported to interact with acidic phospholipid membranes to create functionally stable ATP-dependent cationic pathways.[26] We decided to investigate the interaction between Ago2 and the chaperone HSP90. Immunoprecipitation studies show that when the NP170-PFCE is used to deliver miR, the pull-down of HSP90 brings more Ago2, indicating a closer interaction with its chaperone (Figure 4d). Also, the interaction of Ago2-HSP90 was higher in cells cultured under hypoxia than in normoxia, corroborating the observed increase in the number of Ago2 foci (Figure 4d and Figure 5). These results suggest that the NP170-PFCE is able to serve as a scaffold or to bridge the assembly of more Ago2-HSP90 complexes.

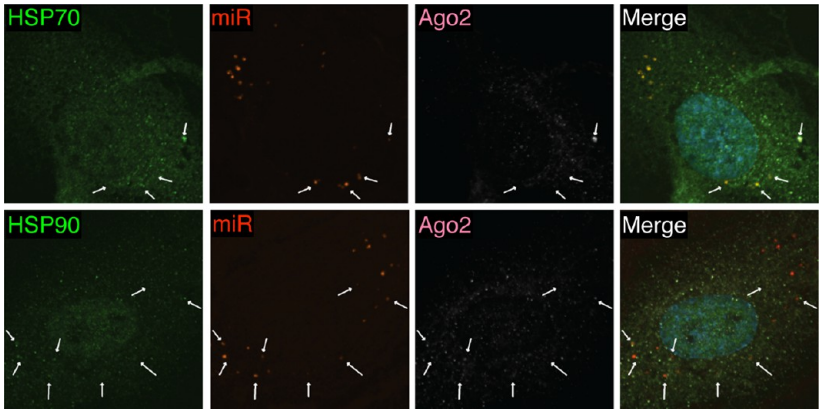

Figure 5. Association between HSPs (HSP70 and HSP90), Ago2, and NP170-PFCE/miR-Dy547. HUVECs were transfected with NP170-PFCE/miR-Dy547 for 4 h, washed to remove NPs that were not internalized, and incubated for 48 h in hypoxia and serum-deprived conditions. Confocal microscopy results show the association of miR-Dy547 with both HSPs and Ago2 protein (arrows).

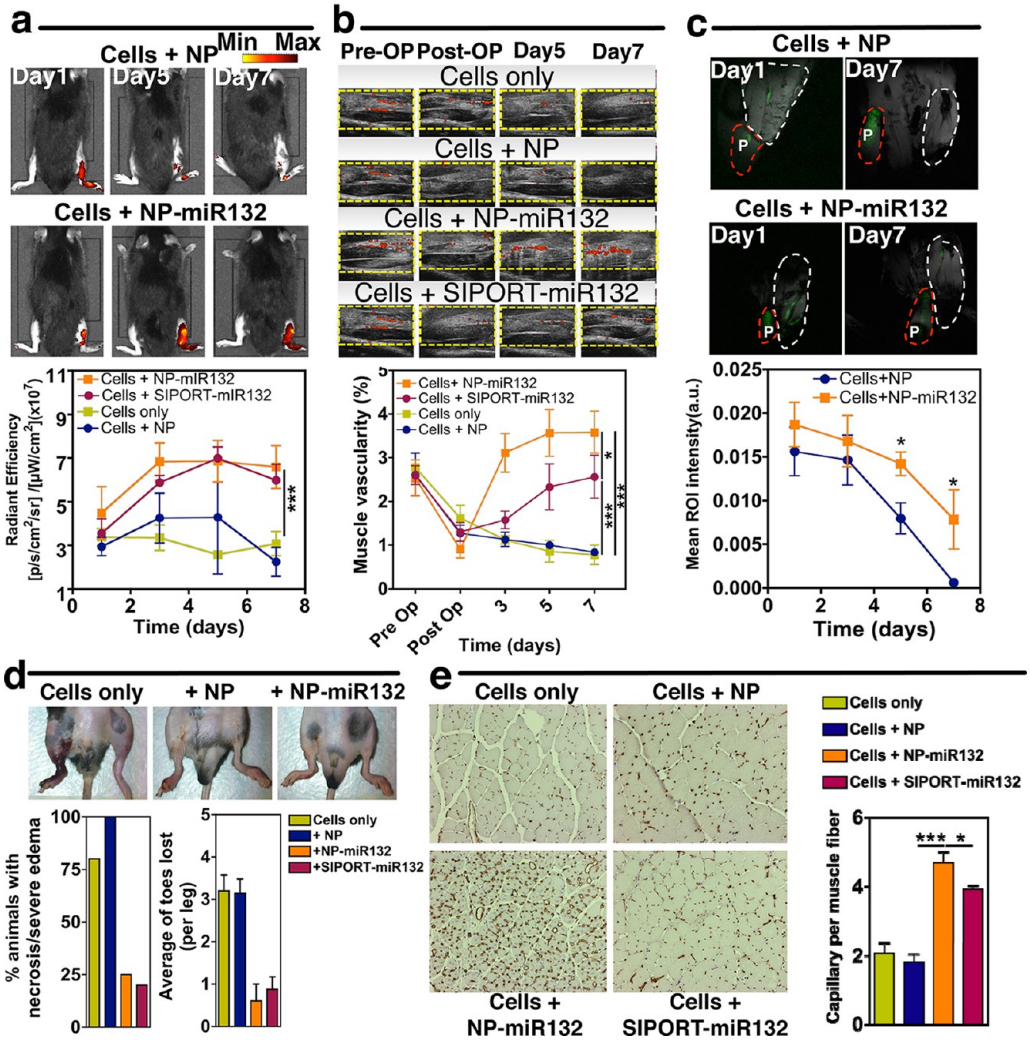

Figure 6. EC survival and angiogenic properties after transfection with NP170-PFCE:miR132 complexes, in a ischemic hindlimb animal model. (a) Representative bioluminescence images and quantified bioluminescence intensity of mice following ligation of the femoral artery and injection of endothelial cells. (b) Representative images and quantification of blood perfusion analyses by VeVo. (c) Representative images and quantification of ^{19}F MRI analysis. The intensity of the region of interest (ROI, in white) of the ^{19}F signal was measured and calibrated against an internal standard (phantom, P, in red). (d) Representative images of ischemic hindlimbs treated with ECs alone or ECs transfected with NP170-PFCE or NP170-PFCE/miR132 and quantification of limb necrosis and loss of toes. Images and quantifications were obtained at day 7. Limbs treated with ECs alone or transfected with NP170-PFCE show a high sign of necrosis. Limbs treated with ECs transfected with NP170-PFCE/miR132 or SIPORT/miR132 have low signs of necrosis. (e) Immunohistochemical staining for CD31 and quantification of capillaries per muscle fiber at 7 days after ligation for the various experimental groups. In all graphs, values are average ± SEM ($n = 4-8$). $p \leq 0.05$ (*), $p \leq 0.01$ (**), and $p \leq 0.001$ (***).

***In Vivo* Monitoring and Activity of NP170-PFCE-miR132-Transfected ECs in a Hind Limb Ischemia Animal Model.** Next, the potential for NP170-PFCE/miR132 to enhance EC survival and promote neovascularization in an *in vivo* model of hindlimb ischemia was investigated. Mouse ECs labeled with a 1,1′-dioctadecyl-3,3,3′,3′-tetramethylindotricarbocyanine iodide (DiR) fluorescent probe were transfected with NP170-PFCE/miR132 for 4 h, washed, and injected in mice legs following ligation of the right femoral artery. Survival of the transplanted cells was assessed using a bioluminescence imaging system (IVIS), allowing evaluation of the spatiotemporal kinetics of EC survival. ECs transfected with NP170-PFCE-miR132 or SIPORT-miR132 proliferated by day 3, as confirmed by an increase in the radiant efficiency. At day 7, the number of cells transfected with NP170-PFCE-miR132 was 3-fold higher ($p < 0.001$, $n = 5$) than with NP170-PFCE without miR132 or cells alone (Figure 6a).

The bioluminescence results were confirmed by evaluation of blood perfusion using a VeVo system (Figure 6b), which was also able to ensure an effective surgical procedure, as shown by a reduction of the blood perfusion in the injured limb. Over time, blood flow increased 2- to 3-fold ($p < 0.001$, $n = 4-8$) in animals treated with cells transfected with NP170-PFCE/miR132 or SIPORT/miR132 compared with animals treated with cells alone or cells labeled with NP170-PFCE without miR132. This increase correlated with cell survival data

attained from IVIS measurements. Importantly, animals treated with NP170-PFCE/miR132 had higher blood perfusion ($p < 0.05$, $n = 4-8$) than animals treated with SIPORT/miR132.

To monitor cell administration and survival, we also used ^{19}F MRI. The intensity of the region of interest (ROI) in ^{19}F MRI images was measured (see Methods section) (Figure 6c). For both experimental groups tested (animals treated with ECs transfected with NP170-PFCE or NP170-PFCE/miR132), there was a decrease in the ^{19}F signal over time. However, after 5 days, animals treated with ECs transfected with NP170-PFCE/miR132 had a higher ^{19}F signal, and thus higher cell number, than animals treated with cells transfected with NP170-PFCE without miR132 ($p < 0.05$, $n = 5, 6$) (Figure 6c).

To further characterize cell engraftment and neovascularization, gross anatomy recordings and histology were performed. Animals treated with ECs alone or cells transfected with NP170-PFCE showed necrotic limbs and autoamputation of toes, while animals treated with NP170-PFCE/miR132 or SIPORT/miR132 showed low signs of necrosis (Figure 6d). The muscles of the injured limbs were further characterized by immunohistochemical staining for CD31 as a marker of ECs and neovascularization. Higher levels of CD31 were observed in animals treated with ECs transfected with NP170-PFCE/miR132 as compared to cells transfected with NPs without miR ($p < 0.001$, $n = 5$) or with SIPORT/miR132 ($p < 0.05$, $n = 5$) (Figure 6e).

Overall, our results show that ECs treated with NP170-PFCE/miR132 have a 3-fold higher survival and pro-angiogenic activity than cells without miRNA in an ischemic hindlimb animal model. To the best of our knowledge this is the first study demonstrating the therapeutic effect of an NP formulation with miR132. Recently the therapeutic activity of miR132 has been shown after the transplantation of saphenous vein-derived pericyte progenitor cells in the infarcted mouse heart, where miR132 released from pericyte progenitor cells stimulated endothelial tube formation by a Ras-dependent induction mechanism, which in turn activated the PI3K/Akt pathway.[27] In our study, animals treated with cells transfected with NP170-PFCE/miR132 had an increase in blood perfusion, correlating with an increase in the near-infrared signal using IVIS and a decrease of signal in ^{19}F MRI. Furthermore, immunohistochemistry results show a 2.5-fold increase in the number of cells expressing the endothelial marker CD31, indicative of neo-angiogenesis. Importantly, ECs transfected with NP170-PFCE/miR132 decreased limb necrosis (4-fold relative to control) and number of toes amputated per leg (6-fold relative to control). The reduction in necrosis is similar to that reported for mouse ischemic limbs treated with genetically modified human mesenchymal stem cells transfected with vascular endothelial growth factor.[28] Furthermore, the percentage of animals without necrotic toes (60%) using cells transfected with NP170-PFCE:miR132 is superior to those treated with endothelial progenitor cells and outgrowth ECs in an alginate scaffold (below 20%).[29]

CONCLUSIONS

In conclusion, we have developed an NP formulation with potential clinical relevance for *in vivo* cell tracking and miRNA delivery. The theranostic aspect of our formulation makes it very promising for cardiovascular applications. We demonstrate that the release of miR132 from the NPs increased by 3-fold the survival of ECs transplanted *in vivo* and 3.5-fold the blood perfusion in ischemic limbs relative to control (cells transfected with empty NPs). Although some strategies are being investigated for the intracellular delivery of miRNA in cells, such as liposomes, adeno-associated virus, and lentivirus,[7] some of these strategies (viruses) raise several issues in terms of clinical translation, while others (liposomes) have limitations in stability, versatility, and traceability for miRNA delivery. The formulation reported in this work uses FDA-approved components, which should facilitate its biomedical translation. The formulation can be prepared with controlled size, can incorporate multiple ligands, and can be monitored by ^{19}F MRI. ^{19}F MRI is the ideal tool for noninvasive assessment of cell fate after transplantation, providing positive, quantitative, and background-free contrast. Our formulation is an alternative to superparamagnetic iron oxide NPs currently used in the clinic for MRI applications. Our work further highlights the importance of the targeted intracellular delivery to enhance the efficacy of miRNAs. We show experimental evidence that the miRNA delivery within the endolysosomal compartment offers an excellent opportunity to enhance the biological effect of miRNAs. This creates new opportunities for the development of more effective synthetic formulations for miRNA delivery.

MATERIALS AND METHODS

Preparation of PLGA NPs Containing PFCE. Where required, PLGA (Resomers 502 H; 50:50 lactic acid/glycolic acid) (Boehringer Ingelheim) was covalently conjugated to fluoresceinamine (Sigma-Aldrich) according to a protocol reported elsewhere.[30] NPs were prepared by dissolving PLGA (100 mg, optionally labeled with fluoresceinamine) in a solution of dichloromethane/trifluoroethanol (1:8, 6.3 mL) containing perfluoro-1,5-crown ether (PFCE) (100 mg) (Fluorochem, UK). This solution was then added dropwise to a PVA solution (40 mL, 5% w/v in water) and stirred for 3 h. The NPs were centrifuged and washed with distilled water before freeze-drying. Where NPs were coated with PS, NPs (1 mg/mL) and PS (1 mg/mL) were incubated for 10 min under agitation, at room temperature. After the incubation period, the NPs were dialyzed (MWCO of 50 kDa) against distilled water and freeze-dried. Measurement of the

average diameter and amount of fluorine in the NPs was performed as described below.

NP Characterization. Particle size was determined using light scattering *via* a Zeta PALS zeta potential analyzer and ZetaPlus Particle Sizing Software, v. 2.27 (Brookhaven Instruments Corporation). The NPs were suspended in 1 mM potassium chloride buffer pH 5.5 (500 μg/mL) and sonicated for short times (<1 min) before characterization. Size measurements were performed at 25 °C, and data were recorded at a 90° angle, with an equilibration time of 5 min and individual run times of 120 s (5 runs per measurement). The average diameters described in this work are number-weighted average diameters. The zeta potential of NPs was determined in a 1 mM KCl pH 6 solution, at 25 °C. All data were recorded with at least 6 runs with a relative residual value (measure of data fit quality) of 0.03.

Quantification of Fluorine in NPs and NP-Labeled Cells by ^{19}F NMR. ^{19}F NMR analyses were performed in a 600 MHz NMR Varian Instrument. NPs (5 mg) were dissolved in dichloromethane (300 μL) and transferred to a 5 mm NMR tube containing a sealed 3 mm tube with trifluoroacetic acid and ^{1}H-dichloromethane as an internal reference. A total of 50 averages were run, with pulses at a 90° angle after a relaxation time of 15 s. Batches of 2×10^6 cells/condition were labeled with NPs (between 0.5 and 8 mg/mL) for 4 h in serum-free EGM-2 (HUVECs) or serum-free M199 (MNCs). After incubation, HUVECs were washed three times with PBS and trypsinized (0.2% trypsin), while MNCs were washed three times with PBS and then passed through a MACS column (Miltenyi Biotec) to further separate the cells from the noninternalized NPs. At the end, all cells were counted with trypan blue, resuspended in PBS, frozen at 80 °C, and freeze-dried. The lyophilized cells were then dissolved in ^{1}H-dichloromethane (300 μL), transferred to a 5 mm NMR tube, and characterized by ^{19}F NMR according to the parameters described previously.

Isolation of Mononuclear Cells from Umbilical Cord Blood (UCB). All human UCB samples were collected from donors, who signed an informed consent form, in compliance with Portuguese legislation. The collection was approved by the ethical committee at Hospital Infante D. Pedro. The samples were stored in sterile bags containing 35 mL of citrate-phosphate-dextrose anticoagulant solution. MNCs were obtained from UCB samples after Ficoll (Histopaque-1077 Hybri Max; Sigma-Aldrich, St. Louis, MO, USA) density gradient separation. MNCs were immediately used for experiments without further treatment.

Complexation of NPs with miRNAs and Cell Transfection. NP170-PFCE were weighed, sterilized under ultraviolet light (UV) light for 30 min, and resuspended in EGM-2 serum-free medium to a final concentration of 500 μg/mL. The NP suspension was dispersed by ultrasound (2×10 s, Branson 2510), and miRs were added (100 or 200 nM, as specified in the text) and allowed to complex to the NPs for 1 h at 37 °C, with intermittent agitation. Cells were washed two times with prewarmed PBS, and the NP170-miR suspension was added to the cells for incubation at 37 °C for 4 h. Cells were transfected at a ratio of 1.25 mg of NP170-miRNA per million HUVEC cells.

For SIPORT (Ambion) transfection, SIPORT transfection agent and miRs were diluted in EGM-2 serum-free medium and incubated at room temperature separately. After 10 min, the solutions were combined and incubated for another 10 min to allow the complexation of both components. The suspension was then dispensed on top of PBS-prewashed cells and incubated for 4 h at 37 °C, as in the NP170 procedure. For visualization of transfection using fluorescence microscopy, NP170-PFCE with fluorescein and miR-Dy547 (Dharmacon) was used. Commercial oligos used in these studies were miR132 (Ambion), miR424 (Ambion), and amiR92a (Exiqon).

FACS Analysis. MNCs (1×10^6 cells) or HUVECs (0.2×10^6 cells) were incubated for 4 h in serum-free M199 or serum-free EGM-2, respectively, containing variable concentrations of NPs in a 24-well plate. After 4 h, HUVECs were washed with PBS on the plate three times. The cells were then resuspended in serum-free EGM-2, with or without MitoTracker Red CMX-ROS at 50 nM for 15 min at 37 °C in a CO_2 incubator. The cells were later trypsinized with 0.2% (w/v) trypsin solution, centrifuged at 1000 rpm for 5 min, and fixed with 4% paraformaldehyde for 10 min at room temperature. After fixation they were rewashed and then resuspended in PBS (500 μL), ready for FACS analysis. MNCs were transferred to a 2 mL Eppendorf and centrifuged for 15 min at 20 °C, 1300 rcfs; then cells were further washed by using anti-CD45 human microbeads *via* a Miltenyi Biotec Mini MACS system and protocol (Miltenyi Biotec, UK) to ensure that only MNCs were present in the final solution and no free NPs. The cells were then incubated with MitoTracker (50 nM) for 15 min at 37 °C, washed once with PBS, and fixed with 4% paraformaldehyde for 10 min at room temperature. After fixation, the cells were washed and resuspended in 500 μL of PBS before FACS analysis. A total of 80 000 events were recorded per measurement.

Confocal Microscopy Analyses. Cells were seeded onto circular 20 mm glass coverslips, coated with 0.2% gelatin inside a 24-well plate, and left to adhere. The cells were then incubated with NPs (500 μg/mL) for 4 h. Once the incubations were terminated, the coverslips were washed gently. In some conditions live cells were stained for lysosomes (using LysoTracker Red DND-99 at 50 nM, 20 min incubation) or mitochondrial activity (using MitoTracker Red CM-Ros, 50 nM, 5 min incubation). Cells were fixed with 4% (w/v, in water) paraformaldehyde (EMS, Hatfield, PA, USA) for 10 min at room temperature and then washed with PBS. For certain conditions, the slides were mounted straight away with mounting medium, 4′,6-diamidino-2-phenylindole (DAPI; Sigma-Aldrich), on a glass slide. Cell membrane staining was also performed. In this case, mouse antibodies against human CD31 (Dako, Glostrup, Denmark) or CD45 (BD Biosciences, Spain) were used to stain the membrane of HUVECs or cord blood mononuclear cells. Cells were washed three times after fixation (MNCs were washed by centrifugation). The cells were then blocked with 2% bovine serum albumin (BSA) (Sigma-Aldrich) in PBS for 30 min at room temperature. The CD31/CD45 (both at 1:50 dilution) primary antibody was added in PBS for 1 h at room temperature followed by three washes in PBS. The binding of primary antibodies was detected with anti-mouse DyLight 649 conjugate (at a dilution of 1:200) (Jackson ImmunoResearch, USA).

Transfection efficiency was evaluated by incubating cells grown on glass coverslips (4 h at 37 °C) with fluorescent miR-Dy547 (control mimic Dharmacon, red) carried by fluorescent NPs (NP-fluorescein, green) or using SiPORT transfection agent. Low-magnification (20× objective, Zeiss laser scanning microscope Meta 510) photographs were taken, observing the need for total signal capture (maximally opening the pinhole) and background normalization. Quantification of the percentage of transfected cells was done by counting the number of miR-DY547 positive cells and compared with the levels of fluorescence in nontransfected cells using ImageJ. Representative microscopic fields were used for quantification spanning a total area of 4.3 mm^2. The total loading per cell was calculated with ImageJ as the "integrated density", which is given by the product between the mean fluorescence intensity and the area of the cell; 200 cells were analyzed in each condition, giving a total area of 0.250 mm^2.

For the intracellular distribution studies, NPs (fluorescein-labeled or unlabeled) or SiPORT complexed with fluorescent oligonucleotides (mimic miRNA transfection control miR-Dy547 (Dharmacon); antagomir-92a fluorescein labeled (Dharmacon)) were incubated with cells for 4 h at 37 °C. Cells were fixed as described above, permeabilized with 0.5% Triton X-100/PBS, and blocked with PBB (2% BSA plus 2% FCS in PBS). Cells were incubated with primary antibodies diluted in PBB according to the manufacturer's instructions and incubated overnight at 4 °C with anti-human argonaute2 (Ago2, 1B1-E2H5 clone active motif, 1:500), RASA1 (1:100), and anti-human GW182 (H70, Santa Cruz Biotechnology sc-66915, 1:100). Other antibodies were incubated for 1 h at room temperature, namely, the early endosomal marker EEA1 (Cell Signaling C45B10, 1:200 dilution) and the late endosome/lysosome marker protein RAB7 (Cell Signaling D95F2, 1:100 dilution). Secondary antibodies were anti-mouse Cy3 (Sigma C2181), anti-rabbit Cy3, and anti-mouse DyLight 649 (Jackson ImmunoResearch). The nucleus of cells was stained with DAPI. After the indirect labeling, high-magnification confocal images (60× objective) were taken, using the optimal pinhole for better discrimination between foci and assuring no overexposure or bleed-through between channels.

Usually images were composed of four channels (blue, green, red, and far-red), where different interactions were analyzed. NPs were green or nonfluorescent depending on how many co-interactions were analyzed; for example, when assessing the association between miR-Dy547/AGO2/GW182 or antagomir-92a/AGO2/GW182 nonfluorescent NPs were used. Images were exported to ImageJ, and analysis was performed with stacks containing the different channels. The interaction of NPs and/or miRs with the different proteins was assessed, considering positive associations to be within 500 nm distance between centers of foci using ImageJ. All the discrete foci (fluorescence levels higher than background) present inside the cell were analyzed by overlaying a ruler of 500 nm length in all directions from the center of each of the foci and scoring the number of foci in the other channels that were contained inside this area; at least 100 cells were analyzed in each condition. Due to the highly variable number of foci present inside the cell (*e.g.*, Ago2 low, EEA1 high, miRs high) we found automated co-localization tools available in ImageJ to be inadequate for this type of analysis.

Immunoprecipitation Studies. For the heat shock protein 90 (anti HSP90, Santa Cruz Biotechnology, SC-59577) pull-down assay, HUVECs growing in 100 mm Petri dishes were trypsinized, washed with PBS, and resuspended in ice cold low-salt lysis buffer (1% Igepal, 50 mM Tris-HCl pH 8) supplemented with a cocktail of proteinase inhibitors. A μMACS Protein A/G Separation kit was used for the immunoprecipitation assay. First, the samples were labeled with the antibody of interest (anti HSP90: 2 μg of antibody per 2 mg of protein in 1 mL of cell lysate). The antibody of interest was captured by addition of protein G MicroBeads (130-071-101 Miltenyi Biotec). Further processing of the samples was performed in accordance with the instructions provided by the manufacturer. Protein quantification was done with a QuantiProTM BCA assay kit (Sigma; QPBCA). The obtained eluates from the microcolumns were loaded in a NuPAGE Novex 3−8% Tris-acetate gel, and the electrophoresis was performed in a XCell SureLock system (~1 h of running time, 150 V with NuPAGE Tris-acetate SDS running buffer). The transfer was done with an Invitrolon PVDF membrane in an XCell II Blot Module (~1 h 30 V with NuPAGE transfer buffer). To detect the interaction of Ago2 with HSP90, the membrane was blocked (30 min in PBS/0.1% Tween 20 (Sigma)/5% low fat milk) and incubated with anti-Ago2 antibody (1:500 in a PBS/0.1% Tween solution; Ago2 Abcam, ab32381) overnight at 4 °C. The membrane was then incubated with specific secondary antibody (anti-rabbit: GE Healthcare Life Sciences). The detection of Ago2 bands was performed by enhanced chemiofluorescence methodology (GE Healthcare Life Sciences) and using a Biorad FX molecular imager system (Bio-Rad). Lane detection and band quantification were done with Image Lab software.

RT-PCR for Gene Expression Profile of Treated Cells. The gene expression profile of specific targets of miR132 was evaluated in HUVECs transfected with NPs, with or without miRNA. Total RNA from experimental groups was isolated using TRIzol (Invitrogen) and an RNeasy Minikit (Qiagen, Valencia). cDNA was prepared from 1 μg total RNA using Taqman reverse transcription reagents (Applied Biosystems, CA, USA). Quantitative PCR (qPCR) was performed using Power SYBR Green PCR Master Mix, and the detection using an ABI PRISM 7500 System (Applied Biosystems). Quantification of target genes was performed relative to the reference gene GAPDH: relative expression = $2[-(Ct_{sample} - Ct_{GADPH})]$. The mean minimal cycle threshold values (Ct) were calculated from quadruplicate reactions. Primer sequences are published in the Supporting Information (Table S4).

Survival and Angiogenesis Assays. After transfection, cells were washed three times with warm PBS and left in complete EGM2 medium overnight. Cells were incubated under low oxygen (0.1%) in serum-deprived conditions for another 48 h. Survival was assessed using the ATP-based assay Cell Titer Glow (Promega) following the manufacturer's instructions. An *in vitro* angiogenesis assay was conducted using IBIDI microangiogenesis slides (IBIDI) and Matrigel (BD) according to the manufacturer's instructions. After 24 h, tube length and number of branching points were measured (blinded analysis) and compared between conditions.

***In Vivo* Studies.** The Experimental Animal Committee of University of Eastern Finland approved all procedures. Unilateral hindlimb ischemia (UHI) was induced by ligating the right femoral artery proximal to the bifurcation of the saphenous and popliteal arteries (by ligation of both femoral artery and vein proximal to the origin of the deep femoral branch) in C57BL/6J male mice (Jackson Laboratory, Bar Harbor, ME, USA). Prior (pre-OP) and after UHI (post-OP) the leg that received the injury was examined using VeVo Doppler to determine the perfusion levels of the femoral artery. Animals were then treated with mouse endothelial cells (MS1 cell line) alone or cells transfected with NP170-PFCE, cells transfected with NP170-PFCE-miR132, or cells transfected with SIPORT-miR132. The cells (5×10^6 cells per animal) were initially labeled with DiR and then suspended in a fibrin gel (50 μL) precursor solution and injected into the gastrocnemius muscle of the operated hindlimb.

Preparation of Mouse Endothelial Cells. The MILE SVEN 1 (MS1) endothelial cell line derived from mouse pancreatic islet was obtained from ATCC (CRL-2279). MS1 cells were cultured in Dulbecco's modified Eagle's medium (DMEM) (Sigma Aldrich) supplemented with fetal bovine serum (5%, FBS) (Biosera) and penicillin−streptomycin solution (1%, Pen/Strep) (Sigma Aldrich). Prior to injection into the animal, the cells were incubated in medium (containing 2% FBS) with NP170-PFCE (500 μg/mL per 400 000 MS1 cells), NP170-PFCE-miR132 (500 μg/mL per 400 000 MS1 cells, 200 nM miRNA), or SIPORT-miR132 (200 nM of miRNA) for 4 h. After cell transfection, cells were washed three times with PBS and then labeled with an IVIS probe for fluorescence detection using near-infrared lipophilic carbocyanine dye denoted by 1,1′-dioctadecyl-3,3,3′,3′-tetramethylindotricarbocyanine iodide (1.75 μg/mL dye in PBS per 5×10^6 cells; the incubation was done for 30 min at 37 °C, as recommended by the vendor (Caliper Life Sciences)). The cells were then washed with PBS, trypsinized, and centrifuged. The pellet was resuspended in a fibrin gel (50 μL); the solution was placed in a 1 mL diabetic syringe and kept on ice until needed for injection into the animals. For injection, 5×10^6 cells were prepared per syringe for injection in the mouse hindlimb.

The fibrin gels were made by cross-linking fibrinogen in the presence of thrombin (both from Sigma-Aldrich). The fibrinogen solution was prepared by dissolving human fibrinogen in Tris-buffered saline (TBS) (Sigma-Aldrich), pH 7.4 (20 mg/mL), and then sterilized by filtering through a 0.22 μm syringe filter (Acrodisc, Pall). Fresh thrombin solutions were prepared by dissolving human thrombin in TBS at pH 7.4 at a concentration of 50 U/mL. Fibrin gels (50 μL, unless otherwise stated) were prepared by mixing three different components: fibrinogen (10 mg/mL), $CaCl_2$ (Merck, NJ, USA) (2.5 mM), and thrombin (2 U/mL).

***In Vivo* Imaging System (IVIS) Analysis.** Animals were imaged under isofluorane anesthesia, at days 1, 3, 5, and 7 postsurgery. IVIS was performed to image the transplanted cells using IVIS Lumina II hardware (Caliper Life Sciences). A laser with the values for far-red Cy5 imaging at a 640 nm excitation and 670 nm emission filter was used; after an exposure time of 0.5 s images were obtained. The imaging field was 12.5 × 12.5 cm.

VeVo Analysis. Ischemic gastrocnemius muscle perfusion was measured on day 0 (pre- and postoperative) and day 3, 5, and 7 after surgery. Perfusion data were acquired with a high-resolution imaging system (Vevo 770, VisualSonics Inc., Toronto, ON, Canada), using an ultrasound probe (RMV-704) in Power Doppler mode (power 100%, RF-cycle 5, gain 25, velocity medium, wall filter 15, scan speed 15, priority 100, intensity range maximum 53 and minimum 19). Video clips containing approximately 50 frames were captured, and the vascularity index (normalized to the area of the muscle) in three evenly separated frames was quantified with VeVo 770 measurement software (VisualSonics). The results are represented as group means of ratios to intact values to reduce measurement-dependent variation.

^{19}F/^{1}H *in Vivo* MRI. MRI analysis was performed using a 9.4 T horizontal bore (60 G/cm, inner bore diameter 120 mm) system (Varian), using a Direct Drive console (VJ NMR) with a linear transmit and receiver, on animals 1, 3, 5, and 7 days postsurgery. ^{19}F MRI was performed to detect NP-labeled cells, while ^{1}H MRI

was done for anatomy of the limbs. ^{19}F MR images were acquired using a custom-built circular surface coil tunable to ^{19}F. Mice were anesthetized by the use of isoflurane (4%) in oxygen (100%) and placed in a custom-built cradle for horizontal positioning in the magnet bore. Maintenance anesthesia was 1.5−2% isoflurane at 1 L min^{-1} oxygen flow. For ^{1}H imaging, coronal GEMS images of the legs were taken at a matrix size of 128 (later zero-filled to 256), 30 averages, field of view 35 × 35 cm, 10 imaging planes of 1 mm depth, TE/TR = 4/1.2 ms with a flip angle of 70°. The ^{1}H images were later isotropically zero-filled by a factor of 2 and filtered (modified third-order Butterworth filter) before Fourier transformation. For ^{19}F imaging, coronal GEMS images of the legs cloned from the ^{1}H images were taken at a matrix size of 256, 60 averages, field of view 35 × 35 cm, 1 imaging plane of 10 mm depth, TE/TR = 4/1.2 ms with a flip angle of 90°. All images were Fourier transformed and overlaid. At all times a phantom, denoted P, was present to allow shimming and pulse calibration and to aid orientation within the surface coil.

Postmortem Histological Analysis. The animals were sacrificed 7 days postsurgery. The mice were perfused with PFA (1%) in citrate buffer through the abdominal aorta, and the test muscle was excised and fixed with 4% PFA in 7.5% sucrose for 4 h. Sections (4 μm) were immunostained with rat anti-mouse CD31 antibody (dilution 1:25, MEC 13.3; BD Biosciences Pharmingen, San Diego, CA, USA). As a secondary antibody, biotinylated rabbit anti-rat antibody (Vector Laboratories, Burlingame, CA, USA) was used and detected using the avidin−biotin−horseradish peroxidise system (Vector Laboratories, CA, USA) with DAB as a chromogen (Zymed, San Francisco, CA, and tyramide signal amplification system (TSA, Biotin System, PerkinElmer, Shelton, CT, USA). Photographs of the stained sections were taken and processed using an Olympus AX70 microscope (Olympus Optical, Tokyo, Japan) and analySIS imaging software (Soft Imaging System GmbH, Muenster, Germany), respectively. Capillary density (capillary/muscle fiber ratios) was measured from three microscopic fields of CD31 immunostained sections taken in close proximity to the needle track at 100× magnification in a blinded manner.

Conflict of Interest: The authors declare no competing financial interest.

Acknowledgment. We thank Dr. Jeffrey Karp and Dr. Michael Goldberg for critical review of the manuscript. This work was supported by a Marie Curie-Reintegration Grant (FP7-People-2007-4-3-IRG; contract no. 230929), MIT-Portugal program, British Heart Foundation Programme Grant (RG/07/004/22659), and FCT (PTDC/CTM/099659/2008 and SFRH/BD/33466/2008, a fellowship to R.S.M.G.).

Supporting Information Available: Supplementary figures. This material is available free of charge *via* the Internet at http://pubs.acs.org

REFERENCES AND NOTES

1. Haider, H.; Ashraf, M. Strategies to Promote Donor Cell Survival: Combining Preconditioning Approach with Stem Cell Transplantation. *J. Mol. Cell Cardiol.* **2008**, *45*, 554–566.
2. Ferreira, L.; Pedroso, D. C.; Vazao, H.; Gomes, R. S. Stem Cell-Based Therapies for Heart Regeneration: What Did the Bench Teach Us? *Cardiovasc. Hematol. Disord. Drug Targets* **2010**, *10*, 173–185.
3. Hu, S.; Huang, M.; Nguyen, P. K.; Gong, Y.; Li, Z.; Jia, F.; Lan, F.; Liu, J.; Nag, D.; Robbins, R. C.; *et al.* Novel Microrna Prosurvival Cocktail for Improving Engraftment and Function of Cardiac Progenitor Cell Transplantation. *Circulation* **2011**, *124*, S27–34.
4. Bonauer, A.; Carmona, G.; Iwasaki, M.; Mione, M.; Koyanagi, M.; Fischer, A.; Burchfield, J.; Fox, H.; Doebele, C.; Ohtani, K.; *et al.* MicroRNA-92a Controls Angiogenesis and Functional Recovery of Ischemic Tissues in Mice. *Science* **2009**, *324*, 1710–1713.
5. Fasanaro, P.; Greco, S.; Ivan, M.; Capogrossi, M. C.; Martelli, F. MicroRNA: Emerging Therapeutic Targets in Acute Ischemic Diseases. *Pharmacol. Ther.* **2010**, *125*, 92–104.
6. Bartel, D. P. Micrornas: Genomics, Biogenesis, Mechanism, and Function. *Cell* **2004**, *116*, 281–297.
7. Shi, M. A.; Shi, G. P. Intracellular Delivery Strategies for MicroRNAs and Potential Therapies for Human Cardiovascular Diseases. *Sci. Signal.* **2010**, *3*, pe40.
8. Kota, J.; Chivukula, R. R.; O'Donnell, K. A.; Wentzel, E. A.; Montgomery, C. L.; Hwang, H. W.; Chang, T. C.; Vivekanandan, P.; Torbenson, M.; Clark, K. R.; *et al.* Therapeutic Microrna Delivery Suppresses Tumorigenesis in a Murine Liver Cancer Model. *Cell* **2009**, *137*, 1005–1017.
9. Anand, S.; Majeti, B. K.; Acevedo, L. M.; Murphy, E. A.; Mukthavaram, R.; Scheppke, L.; Huang, M.; Shields, D. J.; Lindquist, J. N.; Lapinski, P. E.; *et al.* MicroRNA-132-Mediated Loss of P120rasgap Activates the Endothelium to Facilitate Pathological Angiogenesis. *Nat. Med.* **2010**, *16*, 909–914.
10. Chen, Y.; Zhu, X.; Zhang, X.; Liu, B.; Huang, L. Nanoparticles Modified with Tumor-Targeting scFv Deliver siRNA and miRNA for Cancer Therapy. *Mol. Ther.* **2010**, *18*, 1650–1656.
11. Srinivas, M.; Cruz, L. J.; Bonetto, F.; Heerschap, A.; Figdor, C. G.; de Vries, I. J. Customizable, Multi-Functional Fluorocarbon Nanoparticles for Quantitative in Vivo Imaging Using ^{19}F MRI and Optical Imaging. *Biomaterials* **2010**, *31*, 7070–7077.
12. Shi, S. J.; Zhong, Z. R.; Liu, J.; Zhang, Z. R.; Sun, X.; Gong, T. Solid Lipid Nanoparticles Loaded with Anti-MicroRNA Oligonucleotides (AMOS) for Suppression of MicroRNA-21 Functions in Human Lung Cancer Cells. *Pharm. Res.* **2012**, *29*, 97–109.
13. Cheng, C. J.; Saltzman, W. M. Polymer Nanoparticle-Mediated Delivery of Microrna Inhibition and Alternative Splicing. *Mol. Pharm.* **2012**, *9*, 1481–1488.
14. Gibbings, D.; Voinnet, O. Control of RNA Silencing and Localization by Endolysosomes. *Trends Cell Biol.* **2010**, *20*, 491–501.
15. Gibbings, D. J.; Ciaudo, C.; Erhardt, M.; Voinnet, O. Multivesicular Bodies Associate with Components of miRNA Effector Complexes and Modulate miRNA Activity. *Nat. Cell Biol.* **2009**, *11*, 1143–1149.
16. Paulo, C. S.; Pires das Neves, R.; Ferreira, L. S. Nanoparticles for Intracellular-Targeted Drug Delivery. *Nanotechnology* **2011**, *22*, 494002.
17. Ahrens, E. T.; Flores, R.; Xu, H.; Morel, P. A. In Vivo Imaging Platform for Tracking Immunotherapeutic Cells. *Nat. Biotechnol.* **2005**, *23*, 983–987.
18. Partlow, K. C.; Chen, J.; Brant, J. A.; Neubauer, A. M.; Meyerrose, T. E.; Creer, M. H.; Nolta, J. A.; Caruthers, S. D.; Lanza, G. M.; Wickline, S. A. ^{19}F Magnetic Resonance Imaging for Stem/Progenitor Cell Tracking with Multiple Unique Perfluorocarbon Nanobeacons. *FASEB J.* **2007**, *21*, 1647–1654.
19. Mignion, L.; Magat, J.; Schakman, O.; Marbaix, E.; Gallez, B.; Jordan, B. F. Hexafluorobenzene in Comparison with Perfluoro-15-Crown-5-Ether for Repeated Monitoring of Oxygenation Using 19F MRI in a Mouse Model. *Magn. Reson. Med.* **2013**, *69*, 248–254.
20. Luo, D.; Saltzman, W. M. Synthetic DNA Delivery Systems. *Nat. Biotechnol.* **2000**, *18*, 33–37.
21. Ferreira, L.; Karp, J. M.; Nobre, L.; Langer, R. New Opportunities: The Use of Nanotechnologies to Manipulate and Track Stem Cells. *Cell Stem Cell* **2008**, *3*, 136–146.
22. Arbab, A. S.; Yocum, G. T.; Kalish, H.; Jordan, E. K.; Anderson, S. A.; Khakoo, A. Y.; Read, E. J.; Frank, J. A. Efficient Magnetic Cell Labeling with Protamine Sulfate Complexed to Ferumoxides for Cellular MRI. *Blood* **2004**, *104*, 1217–1223.
23. Ghosh, G.; Subramanian, I. V.; Adhikari, N.; Zhang, X.; Joshi, H. P.; Basi, D.; Chandrashekhar, Y. S.; Hall, J. L.; Roy, S.; Zeng, Y.; *et al.* Hypoxia-Induced microRNA-424 Expression in Human Endothelial Cells Regulates HIF-α Isoforms and Promotes Angiogenesis. *J. Clin. Invest.* **2010**, *120*, 4141–4154.
24. Huang, J. G.; Leshuk, T.; Gu, F. X. Emerging Nanomaterials for Targeting Subcellular Organelles. *Nanotoday* **2011**, *6*.
25. Iwasaki, S.; Kobayashi, M.; Yoda, M.; Sakaguchi, Y.; Katsuma, S.; Suzuki, T.; Tomari, Y. Hsc70/Hsp90 Chaperone Machinery

Mediates ATP-Dependent RISC Loading of Small RNA Duplexes. *Mol. Cell* **2010**, *39*, 292–299.
26. Arispe, N.; De Maio, A. ATP and ADP Modulate a Cation Channel Formed by Hsc70 in Acidic Phospholipid Membranes. *J. Biol. Chem.* **2000**, *275*, 30839–30843.
27. Katare, R.; Riu, F.; Mitchell, K.; Gubernator, M.; Campagnolo, P.; Cui, Y.; Fortunato, O.; Avolio, E.; Cesselli, D.; Beltrami, A. P.; *et al*. Transplantation of Human Pericyte Progenitor Cells Improves the Repair of Infarcted Heart through Activation of an Angiogenic Program Involving MicroRNA-132. *Circ. Res.* **2011**, *109*, 894–906.
28. Yang, F.; Cho, S. W.; Son, S. M.; Bogatyrev, S. R.; Singh, D.; Green, J. J.; Mei, Y.; Park, S.; Bhang, S. H.; Kim, B. S.; *et al*. Genetic Engineering of Human Stem Cells for Enhanced Angiogenesis Using Biodegradable Polymeric Nanoparticles. *Proc. Natl. Acad. Sci. U.S.A.* **2010**, *107*, 3317–3322.
29. Silva, E. A.; Kim, E. S.; Kong, H. J.; Mooney, D. J. Material-Based Deployment Enhances Efficacy of Endothelial Progenitor Cells. *Proc. Natl. Acad. Sci. U.S.A.* **2008**, *105*, 14347–14352.
30. Horisawa, E.; Kubota, K.; Tuboi, I.; Sato, K.; Yamamoto, H.; Takeuchi, H.; Kawashima, Y. Size-Dependency of DL-Lactide/Glycolide Copolymer Particulates for Intra-Articular Delivery System on Phagocytosis in Rat Synovium. *Pharm. Res.* **2002**, *19*, 132–139.